JACS
JOURNAL OF THE AMERICAN CHEMICAL SOCIETY
Article
pubs.acs.org/JACS

Gradient Crystallization-Driven Self-Assembly: Cylindrical Micelles with "Patchy" Segmented Coronas via the Coassembly of Linear and Brush Block Copolymers

John R. Finnegan,[†,§] David J. Lunn,[†,§] Oliver E. C. Gould,[†] Zachary M. Hudson,[†] George R. Whittell,*[,†] Mitchell A. Winnik,*[,‡] and Ian Manners*[,†]

[†]School of Chemistry, University of Bristol, Bristol BS8 1TS, United Kingdom
[‡]Department of Chemistry, University of Toronto, Toronto, Ontario M5S 3H6, Canada

Supporting Information

ABSTRACT: Block copolymers (BCPs) with a short crystallizable poly(ferrocenyldimethylsilane) (PFS) core-forming block self-assemble in selective solvents to afford cylindrical micelles, the ends of which are active to further growth via a process termed living crystallization-driven self-assembly (CDSA). We now report studies of the CDSA of a series of crystalline-brush BCPs with C_6 (**BCP^6**), C_{12} (**BCP^{12}**), and C_{18} (**BCP^{18}**) *n*-alkyl branches that were prepared by the thiol−ene functionalization of PFS-*b*-PMVS (PMVS = poly(methylvinylsiloxane)). Although the increased *n*-alkyl brush length of **BCP^{12}** and **BCP^{18}** hindered micelle growth, the increased intercoronal chain repulsion could be alleviated by their coassembly with linear PFS-*b*-PMVS. When the coassembly was initiated by short cylindrical seed micelles, monodisperse block comicelles of controllable length with "patchy" coronal nanodomains were accessible. TEM and AFM analysis of micelles prepared from **BCP^{18}** and PFS-*b*-PMVS were found to provide complementary characterization in that the OsO_4-stained PMVS coronal domains were observed by TEM, whereas the brush block domains of **BCP^{18}** (which displayed greater height) were detected by tapping mode AFM. The results showed that the coassembly afforded a gradient structure, with an initial bias for the growth of the linear BCP over that of the more sterically demanding brush BCP, which was gradually reversed as the linear material was consumed. This represents the first example of living gradient CDSA, a process reminiscent of a living covalent gradient copolymerization of two different monomers. Although other possible explanations exist, simulations based on a statistical model indicated that the coronal nanodomains detected likely result from a segmented, gradient comicelle architecture that arises as a consequence of: (i) different rates of addition of BCP unimer to the micelle termini, and (ii) a cumulative effect resulting from steric hindrance associated with the brush block.

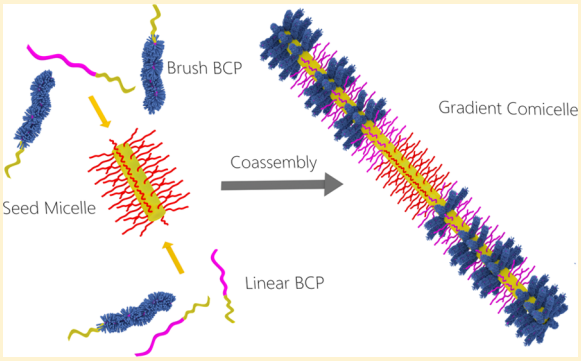

INTRODUCTION

Block copolymers (BCPs) represent ideal building blocks for the creation of a variety of nanoscale objects due to their ability to undergo self-assembly in selective solvents.[1−4] As a result of their morphological diversity, the resulting BCP micelles have found use in a variety of applications, including drug delivery,[5−7] biomedical imaging,[8] composite reinforcement,[9] and as etch resists for surface patterning.[10] Emerging complementary strategies in BCP self-assembly have allowed for the preparation of micelle morphologies exhibiting both complexity and hierarchical order.[11] For example, Janus-type BCP micelles have recently been used as subunits for the preparation of multicompartment micelles and supracolloidal assemblies.[12−14] Similar strategies, where BCPs or blends thereof are self-assembled under kinetic control, can be used to prepare previously inaccessible morphologies.[15,16] In another approach, the polymerization-induced self-assembly (PISA) of amphiphilic BCPs has been used for the preparation of spherical, wormlike, vesicular, and intermediate morphologies.[17−20]

Recently, the self-assembly of crystalline-coil BCPs has allowed access to complex nanoscale architectures that can be prepared with a high degree of dimensional and morphological control. When placed in a selective solvent for the coil block, the self-assembly of these BCPs into micelles is influenced by crystallization of the core-forming block, favoring structures with low interfacial curvature such as cylinders and platelets.[21−24] The preparation of cylindrical and fiber-like micelles by the solution self-assembly of a diverse array of BCPs with crystallizable core-forming blocks has now been reported, including those with polyferrocenylsilane,[25,26] polyethylene,[27−29] poly(ethylene oxide),[30] poly(ε-caprolactone),[31,32] poly(ε-caprolactone-*b*-L-lactide),[33] polylactide,[34−36] polyacrylo-

Received: July 14, 2014
Published: September 22, 2014

 © 2014 American Chemical Society dx.doi.org/10.1021/ja507121h | J. Am. Chem. Soc. 2014, 136, 13835−13844

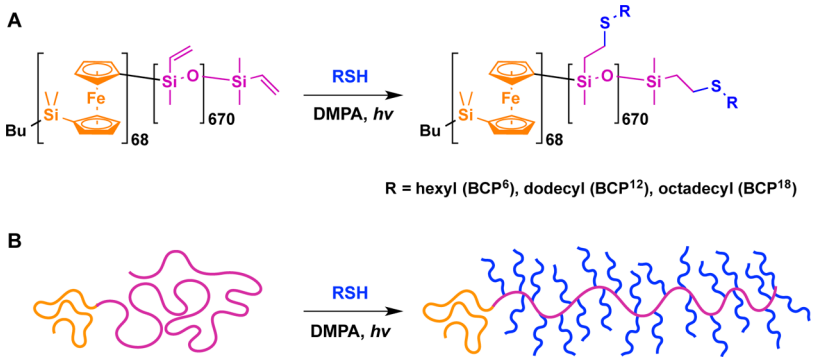

Figure 1. (A) Thiol–ene functionalization of PFS_{68}-*b*-$PMVS_{670}$ with *n*-alkanethiols to prepare brush BCPs using 2,2-dimethoxy-2-phenylacetophenone (DMPA) as a photoinitiator. (B) Schematic representation of the transformation from linear to brush BCP.

nitrile,[37] polyferrocenylgermane,[21] polythiophene[38−45] and liquid crystalline segments.[46,47]

We have previously shown that the termini of micelles with a crystalline poly(ferrocenyldimethylsilane) (PFS) core are active to further growth via a process termed living crystallization-driven self-assembly (CDSA), which resembles a living covalent polymerization but on a longer length scale.[21,48] For example, monodisperse cylindrical micelles of controlled length can be prepared by adding a known amount of unimer (molecularly dissolved BCP) to a colloidal solution of crystallite seed micelles, prepared by the ultrasonication of long cylindrical micelles.[49] The use of BCPs with the same crystallizable PFS core-forming block but different corona-forming blocks yields "block comicelles", micelle analogues of block copolymers.[21] This approach has been used in recent work on fluorescent multiblock comicelles with potential applications in nanoscale encoding technology.[50] Living CDSA has also been observed for BCPs with different crystallizable core-forming blocks including polyferrocenylgermane,[21] polylactides,[34] polyethylene,[29] and poly(3-hexylthiophene).[38,39,41]

Although the range of nanostructures accessible through living CDSA has increased significantly in recent years, several limitations remain.[51] For example, the development of controlled methods for preparing BCP micelles with "patchy" compartmentalized coronal domains remains a challenge. Recently, Schmalz and workers reported the preparation of BCP micelles with compartmentalized polystyrene/poly(methyl methacrylate) (PS/PMMA) coronas and a crystalline polyethylene (PE) core from triblock terpolymers.[28,29,52] B-A-B block comicelles were formed from cylindrical seeds of PS-*b*-PE-*b*-PS by the addition of PS-*b*-PE-*b*-PMMA unimer. For the B segments of the comicelles formed from the triblock terpolymer, a patch-like corona was observed due to phase-separation of the two incompatible (large χN) PS and PMMA corona-forming blocks.

We have previously attempted to obtain nanophase coronal segregation in PFS-based cylindrical micelles by adding blends of PFS-*b*-PI (PI = polyisoprene) and PFS-*b*-PDMS (PDMS = poly(dimethylsiloxane)) unimers to PFS-*b*-PI seed micelles.[53] Because of the large χN for the two corona-forming blocks, we anticipated that the micelle corona would consist of phase-segregated PI and PDMS domains. Surprisingly, however, no coronal segregation could be detected by TEM in this case, even after selective staining of the PI blocks with OsO_4. Another interesting feature of these experiments is that they showed that the coronal chains influence the packing density of BCP molecules in the micelles, as demonstrated by pronounced differences in the number of BCP molecules per nanometer; a property that we refer to as the linear aggregation number, $N_{agg,L}$.[53]

Herein, we report the synthesis and living CDSA of a series of PFS-based brush BCPs. By exploiting the coassembly of linear and brush BCPs and their inherently different growth rates, we now describe the successful preparation of monodisperse cylindrical micelles where segregation of coronal domains is observed and where the domain size can be influenced by the size and amount of brush BCP used. Moreover, our studies provide valuable new insight into the living CDSA process and the key role played by the coronal block at the termini of the growing micelles and that of the incoming unimer.

■ RESULTS

1. Synthesis and Characterization of Brush BCPs. Inspired by recent work on brush BCP self-assembly,[54−57] we targeted an exploration of the ability of brush BCPs containing a crystalline PFS core-forming block to participate in CDSA. The diblock copolymers PFS_{63}-*b*-$PDMS_{513}$ and PFS_{68}-*b*-$PMVS_{670}$ were prepared by sequential living anionic polymerization of dimethylsila[1]ferrocenophane and hexamethylcyclotrisiloxane or 1,3,5-trimethyl-1,3,5-trivinylcyclotrisiloxane, respectively (Table S1, Supporting Information). By adapting a recently reported method,[58] brush BCPs with *n*-hexyl (**BCP^6**), *n*-dodecyl (**BCP^{12}**), and *n*-octadecyl (**BCP^{18}**) side-chain branches were prepared by photoinitiated thiol–ene functionalization of PFS_{68}-*b*-$PMVS_{670}$ with *n*-alkanethiols (Figure 1). The resulting series of BCPs consisted of a semicrystalline PFS core-forming block and a bottlebrush polysiloxane corona-forming block with *n*-alkyl side chains composed of 6, 12, and 18 carbon atoms. Quantitative conversion of vinyl groups was confirmed by ^{1}H, ^{13}C, and ^{29}Si NMR spectroscopy. Each brush BCP was isolated in high yield (Table S2, Supporting Information) and an increase in hydrodynamic size was observed by GPC, with the retention time of the brush BCPs decreasing with increasing side chain length (Figure S1, Supporting Information).

2. CDSA of Brush BCPs. To determine the effect of a bottlebrush corona-forming block on CDSA, cylindrical micelles were grown from each of the brush BCPs. Concentrated unimer solutions of **BCP^6**, **BCP^{12}**, and **BCP^{18}** were prepared in THF (10 mg·mL^{-1}), a good solvent for both blocks. Equimolar amounts of each brush BCP unimer were added to separate vials containing freshly prepared PFS_{63}-*b*-$PDMS_{513}$ seed micelles (L_n = 120 nm, L_w/L_n = 1.38, Figure S5,

Supporting Information) in *n*-hexane (0.05 mg·mL^{-1}) (Figure 2). For comparison, micelles were also prepared by the seeded growth of PFS_{68}-*b*-$PMVS_{670}$ unimer under the same conditions. The growth of each sample was monitored by transmission electron microscopy (TEM) after solvent evaporation over a period of 4 weeks.[59]

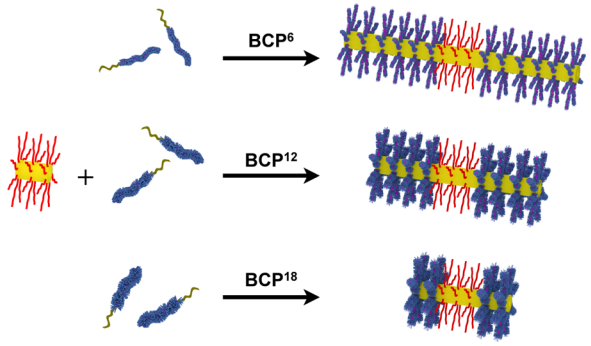

Figure 2. Schematic representation of cylindrical micelles prepared by growth of an equimolar amount of **BCP**^{6}, **BCP**^{12}, and **BCP**^{18} unimers (blue corona) from PFS_{63}-*b*-$PDMS_{513}$ seed micelles (red corona).

Micelles grown from PFS_{68}-*b*-$PMVS_{670}$ reached a mean contour length (L_n) value of 1130 nm (PDI = L_w/L_n = 1.02) after 2 h as determined by statistical analysis of drop-cast micelles imaged by TEM (Figure 3 and S6A). No further growth was detected over the course of the study, consistent with the consumption of all unimer from solution. When unimer of the brush BCP with the shortest side chains, **BCP**^{6}, was added to a solution of seed micelles, the initial rate of growth appeared to be similar to that of linear PFS_{68}-*b*-$PMVS_{670}$, but it took approximately 72 h for the resulting micelles to reach a final L_n value of 1080 nm (L_w/L_n = 1.03, Figure S6B, Supporting Information).[60]

Analogous experiments revealed that **BCP**^{12} and **BCP**^{18} also formed monodisperse cylindrical micelles via seeded growth but also that the rate of self-assembly was significantly lower than that for PFS_{68}-*b*-$PMVS_{670}$ and for **BCP**^{6} (Figure S6C and S6D, Supporting Information). For example, 3 h after the addition of unimer to the seed micelles both BCPs had formed cylindrical micelles with an L_n of 360 nm (L_w/L_n = 1.08). After this point, the rate of self-assembly of the two samples changed (Figure 3A). The addition of **BCP**^{12} to the termini of the growing micelles slowed, resulting in micelles that after 4 weeks had reached a L_n value of 830 nm (L_w/L_n = 1.03) and were still growing (Figure 3B). In contrast, the growth of micelles prepared from **BCP**^{18} almost completely halted, resulting in micelles that after 4 weeks had only increased in length by a further 90 nm to give a L_n value of 450 nm (L_w/L_n = 1.05). Consistent with the presence of excess unimer in the sample containing **BCP**^{18}, large non-uniform film-like regions of high contrast were observed by TEM (Figure S6D). A similar result was obtained for the self-assembly of **BCP**^{18} under homogeneous nucleation conditions.[61] To ascertain whether the excess **BCP**^{18} unimer was still available to add to the termini of the growing micelles, additional seed micelles were added to a sample of the original micelle solution (Figure S7, Supporting Information). However, no growth of the seed micelles was observed over a period of 1 week. To investigate whether the micelles prepared from **BCP**^{18} were still active to further growth, an equimolar amount of either PFS_{68}-*b*-$PMVS_{670}$ (Figure S8, Supporting Information) or **BCP**^{18} (Figure S9, Supporting Information) was added to samples of the original micelle solution. Although in both cases the micelles were observed to continue growing, only the PFS_{68}-*b*-$PMVS_{670}$ unimer appeared to be consumed entirely and micelles prepared by the addition of further **BCP**^{18} unimer only increased by a further 100 nm over a period of 1 week.

3. Coassembly of Brush BCPs and Linear PFS_{68}-*b*-$PMVS_{670}$. As the rate of CDSA of PFS_{68}-*b*-$PMVS_{670}$ was substantially higher than that of **BCP**^{18}, we anticipated that coassembly of the two BCPs could lead to a more efficient CDSA process. We expected that this would allow the formation of cylindrical micelles containing large brush BCP coronas with lengths that were inaccessible by CDSA using seeded growth of **BCP**^{18} alone. Unimers of **BCP**^{18} and of PFS_{68}-*b*-$PMVS_{670}$ were therefore added simultaneously in equimolar amounts to PFS_{60}-*b*-$PDMS_{660}$ seed micelles (L_n = 120 nm, L_w/L_n = 1.38, Figure S5, Supporting Information) in *n*-

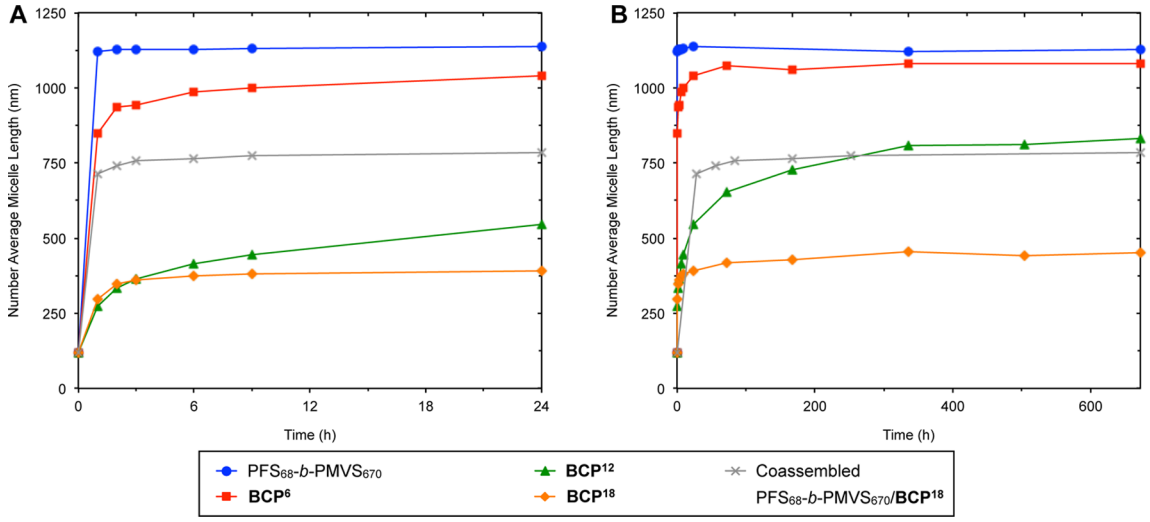

Figure 3. Lengths of PFS_{68}-*b*-$PMVS_{670}$, **BCP**^{6}, **BCP**^{12}, **BCP**^{18}, and coassembled **BCP**^{18} and PFS_{68}-*b*-$PMVS_{670}$ micelles as a function of time, monitored over a period of 9 h (A) and 4 weeks (B) after the addition of unimers to PFS_{63}-*b*-$PDMS_{513}$ seed micelles (L_n = 120 nm, L_w/L_n = 1.38). L_n values (nm) determined by statistical analysis of drop-cast micelles imaged by TEM.

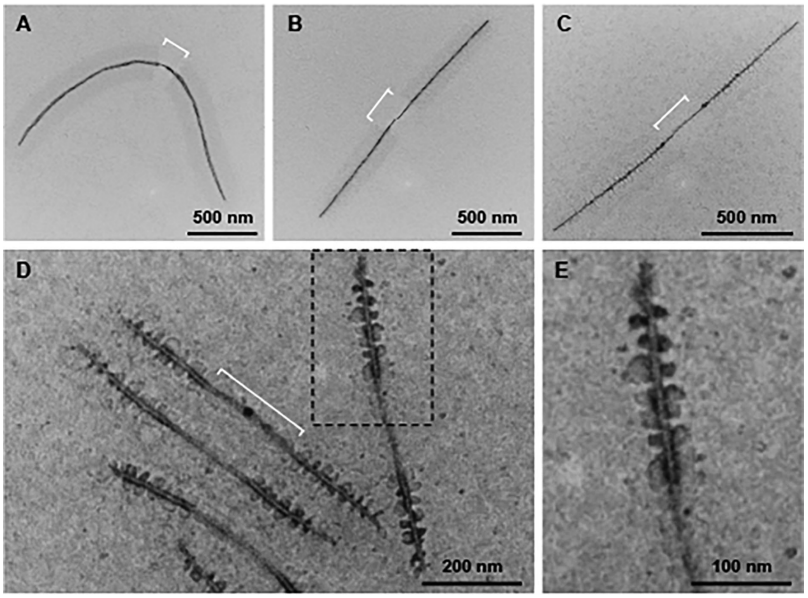

Figure 4. TEM images of OsO_4-stained micelles prepared by the seeded growth of PFS_{68}-*b*-$PMVS_{670}$ (A) and equimolar mixtures of either **BCP**[6] (B), **BCP**[12] (C), or **BCP**[18] (D) and PFS_{68}-*b*-$PMVS_{670}$ from PFS_{60}-*b*-$PDMS_{660}$ seed micelles (L_n = 225 L_w/L_n = 1.07). Seed micelles denoted by white brackets. (E) Enlargement of the dashed line box in D.

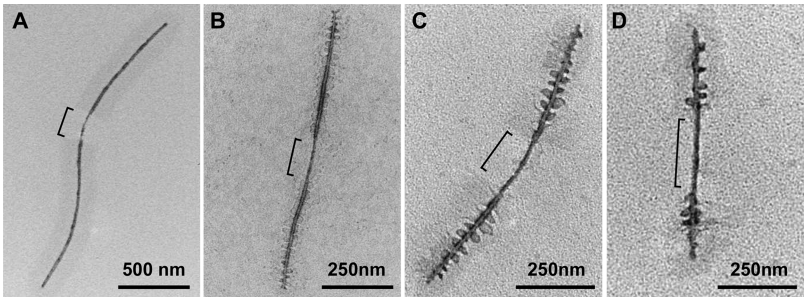

Figure 5. TEM images of OsO_4-stained micelles prepared by the seeded growth of mixtures of **BCP**[18] and PFS_{68}-*b*-$PMVS_{670}$ from PFS_{60}-*b*-$PDMS_{660}$ seed micelles (L_n = 225 L_w/L_n = 1.07). Seed micelles denoted by black brackets. Mole ratios (**BCP**[18]:PFS_{68}-*b*-$PMVS_{670}$) of 0:100 (A), 20:80 (B), 50:50 (C), and 80:20 (D).

hexane (0.05 mg·mL^{-1}). TEM analysis of the evolution of the CDSA process showed a significant increase in the rate of cylinder growth during the first 2 h after the addition of the two unimers relative to the rate of CDSA of **BCP**[18] unimer alone. From this point onward the rate of CDSA slowed significantly and was comparable to that of the seeded growth of **BCP**[18] unimer alone, resulting in cylindrical micelles with a L_n value of 850 nm (L_w/L_n = 1.03) 4 weeks after the addition of unimers (Figure 3).

To identify the composition of the corona of these micelles and gain a better understanding of the coassembly of brush and linear BCPs, unimers of **BCP**[6], **BCP**[12], or **BCP**[18] and of PFS_{68}-*b*-$PMVS_{670}$ were added simultaneously in equimolar amounts to longer monodisperse PFS_{60}-*b*-$PDMS_{660}$ seed micelles (L_n = 225 nm, L_w/L_n = 1.07, Figures S10 and S11, Supporting Information) and the resulting colloidal solutions aged for 1 week. For comparison, unimers of only PFS_{68}-*b*-$PMVS_{670}$ were also added to the seed micelles to prepare micelles with coronas composed entirely of PMVS. Drop-cast samples of the resulting micelle solutions were exposed to OsO_4 vapor to selectively stain the vinyl groups of the PMVS corona-forming block. After staining, TEM images of micelles prepared exclusively by the seeded growth of PFS_{68}-*b*-$PMVS_{670}$ unimer showed no evidence of coronal segmentation (Figure 4A, and Figure S12A, Supporting Information). Furthermore, the PFS core of the micelle and the PMVS corona could clearly be observed as regions of high and intermediate contrast, respectively. TEM images of micelles containing **BCP**[6] and PFS_{68}-*b*-$PMVS_{670}$ also showed no evidence of coronal segmentation and as such were almost indistinguishable from micelles composed of solely PFS_{68}-*b*-$PMVS_{670}$ (Figure 4B, and Figure S12B, Supporting Information). However, TEM images of the micelles containing a mixture of either **BCP**[12] or **BCP**[18] and PFS_{68}-*b*-$PMVS_{670}$ showed segmented areas of high and low electron density in the coronas of the micelles, representing regions of stained and unstained corona respectively (Figure 4C, 4D, 4E, and Figure S12C, Supporting Information). Furthermore, in the case of **BCP**[18] it can be seen that the size of the PMVS patches decreases with increasing distance from the seed. When comparing the two larger brush BCPs, the size and definition of the different coronal domains increased in the samples prepared from **BCP**[18] as compared to those prepared from **BCP**[12]. As the PFS_{60}-*b*-$PDMS_{660}$ seed micelles contained no vinyl groups, they could be clearly observed in all of the TEM images as a distinct break in the coronal staining. This emphasizes the efficiency of OsO_4 as a staining agent to

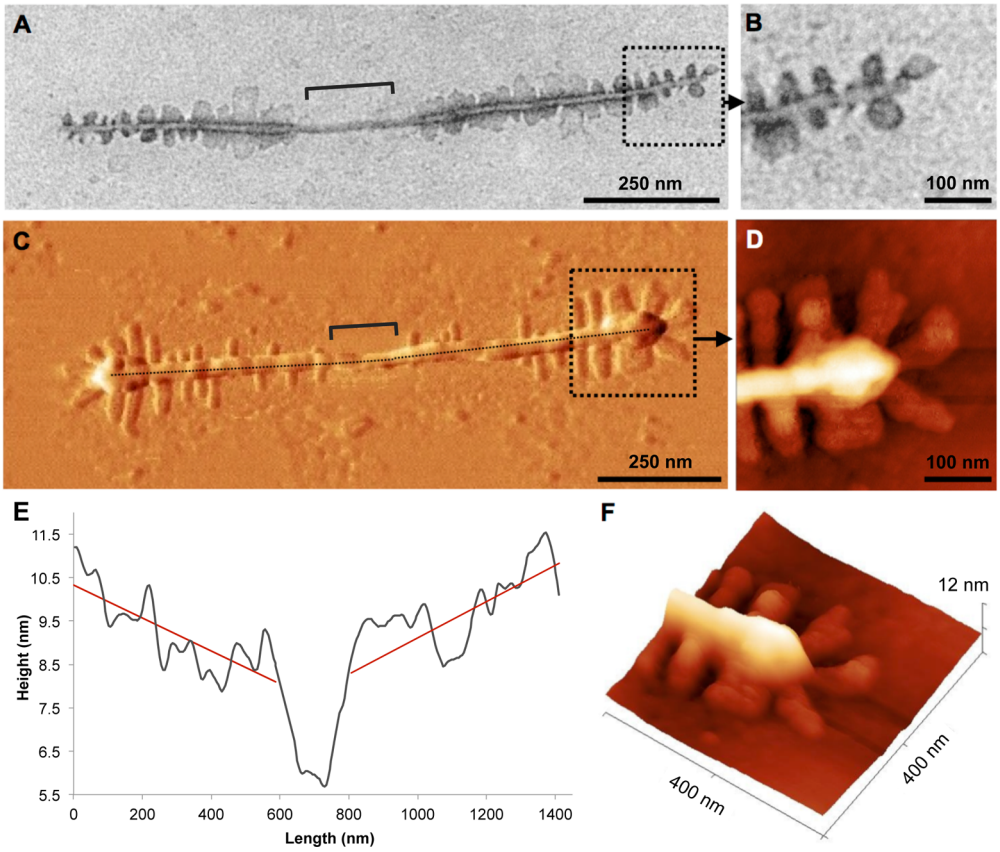

Figure 6. Representative TEM images of an OsO_4-stained micelle prepared by the seeded growth of **BCP**[18] and PFS_{68}-*b*-$PMVS_{670}$ (20:80 mol ratio) from PFS_{60}-*b*-$PDMS_{660}$ seed micelles (L_n = 225 L_w/L_n = 1.07) (A and B). Seed micelles denoted by black brackets. AFM phase (C) and height (D) images of a similarly representative micelle spin-coated onto mica. (E) AFM height profile along the dashed line in C (red trend lines show height increase toward the termini of the coassembled micelle). (F) 3D view of AFM height image in D.

selectively increase the contrast of only the PMVS corona-forming block.

As a control experiment, micelles were also prepared by the seeded growth of an equimolar mixture of PFS_{68}-*b*-$PMVS_{670}$ and PFS_{63}-*b*-$PDMS_{513}$ unimers from the 225 nm PFS_{60}-*b*-$PDMS_{660}$ seed micelles (Figure S13, Supporting Information). The sample was aged for 1 week, and drop-cast samples of the solution were exposed to OsO_4 vapor. After staining, cylindrical micelles with a uniform distribution of the two corona-forming blocks along their lengths were observed by TEM, where the PMVS chains appeared as barely visible, but randomly distributed, fine dark lines (Figure S14, Supporting Information). This suggested that the coronal segmentation detected in the previous examples was an intrinsic feature of the micelles containing **BCP**[12] and **BCP**[18].

4. Controlling the Degree of Coronal Compartmentalization in Micelles Prepared by the Coassembly of BCP[18] and PFS_{68}-*b*-$PMVS_{670}$. In a further series of experiments we sought to determine whether the dimensions of the segmented coronal domains could be controlled by altering the ratio of the brush to linear BCP. Using the system that gave the most obvious coronal compartmentalization, **BCP**[18] and PFS_{68}-*b*-$PMVS_{670}$ unimers were added in different ratios to monodisperse PFS_{60}-*b*-$PDMS_{660}$ seed micelles (L_n = 225 nm, L_w/L_n = 1.07). TEM analysis of the resulting micelles showed a correlation between the size and frequency of the coronal domains and the ratio of the added unimers (Figure 5). Large PMVS domains separated by only small bands of brush BCP were observed for a **BCP**[18] to PFS_{68}-*b*-$PMVS_{670}$ mole ratio of 20:80 (Figure 5B). As the mole fraction of **BCP**[18] was increased, the stained PMVS regions decreased in size and appeared to be more densely packed between larger areas derived from the brush BCP corona (Figure 5D).

In an attempt to detect the different domains of the segmented coronas by atomic force microscopy (AFM), the solution of micelles prepared with a **BCP**[18] to PFS_{68}-*b*-$PMVS_{670}$ mole ratio of 20:80 was spin-coated onto mica. After staining with OsO_4, both amplitude and height images displayed the location of the brush blocks and showed clear coronal segmentation along the length of the micelles (Figure 6). The same coronal segmentation was also apparent when samples were prepared on gold-coated mica without OsO_4 staining (Figure S16, Supporting Information), albeit with lower height contrast between blocks. By TEM the OsO_4-stained PMVS domains within the micelle corona could be observed as regions of high electron density. However, the domains formed from the brush corona of **BCP**[18] could not be directly detected due to the lower electron density of the hydrothiolated polysiloxane block. In contrast, by AFM the brush block coronal domains could be observed due to the increased rigidity and size of the hydrothiolated polysiloxane block. This assertion was confirmed by similarly imaging a micelle that was prepared by the addition of **BCP**[18] alone to the seed micelle. Analysis of the AFM height image (Figure S17, Supporting Information) revealed a maximum value (14 nm) that was more comparable to that of the ends (i.e., brush block

segments) of the coassembled micelle (11.5 nm), rather than the regions approaching the seed (8 nm). A useful feature of the characterization by the two microscopic techniques is that they are complementary: one effectively gives the inverse coronal image of the other. By AFM the seed micelle is observed as a block of reduced height (~6 nm) due to the smaller corona composed entirely of PDMS.

From the TEM images of micelles prepared by the seeded growth of mixtures of **BCP**^{18} and PFS$_{68}$-*b*-PMVS$_{670}$ it is apparent that there is a bias for larger PMVS regions in the corona for the sections of the micelles in close proximity to the seed. Consistent with this observation, the AFM images shown in Figure 6 show larger areas of the sterically bulky corona-forming block of **BCP**^{18} near the micelle termini. In addition, by mapping the height along the center of the cylindrical micelle, an increase is observed as the percentage of the bulkier corona-forming brush block of **BCP**^{18} increases (Figure 6E). This is indicative of preferential consumption of the linear BCP unimer during the initial stages of micelle growth. Thus, as the linear BCP unimer is consumed, the composition of the growing micelles changes in favor of **BCP**^{18}. This leads to a gradient structure in which the average coronal composition reverses along the length of the portion of the micelle that has been grown from the PFS$_{60}$-*b*-PDMS$_{660}$ seed.

■ DISCUSSION

1. Sterically Hindered Micelle Growth for Brush Block Copolymers BCP^{6}, BCP^{12}, and BCP^{18}. Although a growing number of studies of the behavior of crystalline-coil BCPs in coil-selective solvents have been recently reported, very little is known about the influence of the nature and spatial dimensions of the corona-forming block on the self-assembly process. One study showed that PFS block copolymers with longer corona-forming blocks tended to form longer micelles under seeded growth conditions compared to the case involving the addition of an equimolar amount of polymer with a shorter corona block.[53] By grafting *n*-alkyl side chains onto the polysiloxane block of PFS$_{68}$-*b*-PMVS$_{670}$ by thiol−ene "click" chemistry, we were able to prepare a series of related PFS-based crystalline-brush BCPs that have allowed interesting new insight into living CDSA. The increased size of the *n*-alkyl grafted corona-forming blocks was found to reduce the rate of the CDSA process. This was demonstrated by monitoring the seeded growth of PFS$_{68}$-*b*-PMVS$_{670}$, **BCP**^{6}, **BCP**^{12}, and **BCP**^{18} unimers by TEM over a period of 4 weeks (Figure 3). Although micelles formed from either PFS$_{68}$-*b*-PMVS$_{670}$ or **BCP**^{6} grew initially at a fairly similar rate, they reached their final lengths after 2 h and 72 h, respectively. This provided evidence for a significant slowing of the growth in the case of **BCP**^{6} as the micelle became longer. Moreover, seeded growth of **BCP**^{12} and **BCP**^{18} was found to be initially slower than for both PFS$_{68}$-*b*-PMVS$_{670}$ and **BCP**^{6} and to ultimately afford short cylindrical micelles that still appeared to be growing very slowly even after 4 weeks. Our results suggest that the seeded growth of cylindrical micelles from **BCP**^{12} and **BCP**^{18} unimers becomes increasingly slow as the steric bulk of the corona-forming block is increased. We imagine that this cumulative effect arises from the presence of sterically demanding corona-forming blocks in the BCP unimers, leading to a gradual increase in intercoronal chain repulsion as more of such units are incorporated into the growing micelle. This would eventually cause the corona to protrude so far beyond the growing-face of the crystalline core that further unimer addition would be severely hindered, thereby dramatically lowering the rate of CDSA (Figure 7).

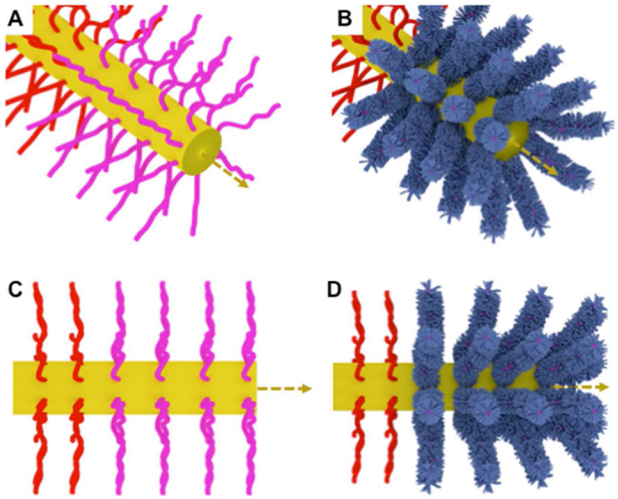

Figure 7. Schematic representation of the termini of micelles prepared by the seeded growth of PFS$_{68}$-*b*-PMVS$_{670}$ (A and C) and **BCP**^{18} (B and D) showing how the accumulation of the increased steric bulk of the corona-forming block of **BCP**^{18} could obscure the crystalline PFS core at the terminus of a cylindrical micelle (red corona = seed micelle; pink corona = PMVS; blue corona = **BCP**^{18}; arrow indicates direction of growth).

In the cases of **BCP**^{12} and **BCP**^{18} the micelle growth was observed to slow to almost a complete halt with substantial amounts of BCP remaining. Interestingly, the remaining brush BCP was found not to undergo homogeneous nucleation to form new micelles under these conditions. However, on addition of linear PFS$_{68}$-*b*-PMVS$_{670}$ unimer, the micelles prepared from **BCP**^{18} were observed to increase in length, showing that the micelle termini remain active to further growth (Figure S8, Supporting Information). When further **BCP**^{18} unimer was added instead, the micelles prepared from **BCP**^{18} were also observed to increase in length. However, the micelles only grew by ~100 nm over a period of 1 week and the cores were observed to taper toward their ends (Figure S9, Supporting Information). It is possible that unimers of **BCP**^{18} may evolve into kinetically trapped unimolecular micelles that are stabilized by the large brush corona-forming block or non-uniform aggregates. To test this idea, additional seed micelles were added to a sample composed of **BCP**^{18} micelles but for which growth had slowed and unattached BCP remained in solution. Over a period of 1 week, no growth of the seeds was observed, suggesting that the BCP still present in the solution is unavailable to add to the termini of either the pre-existing **BCP**^{18} micelles or the additional seed micelles (Figure S7, Supporting Information).

2. Formation of Gradient Micelle Structures by Coassembly. We found that addition of a mixture of **BCP**^{18} together with linear PFS$_{68}$-*b*-PMVS$_{670}$ to a solution of seed micelles increased the rate of self-assembly of the larger brush BCP and allowed longer micelles to be obtained. The presence of the linear BCP appears to relieve intercoronal chain repulsion and prevent coronal crowding effects at the micelle termini caused by repeated addition of the brush BCP. Interestingly, analysis of the length of micelles prepared by the coassembly of **BCP**^{18} and PFS$_{68}$-*b*-PMVS$_{670}$ as a function of

time showed two distinct rates of CDSA (Figure 3). After the addition of the unimer mixture the initial rate of micelle growth was comparable to that for the CDSA of PFS_{68}-*b*-$PMVS_{670}$ unimer alone. However, after 2 h the rate of micelle growth slowed rapidly to become comparable to that of the CDSA of **BCP**[18] unimer alone, although the length obtained (ca. 830 nm) far exceeded that observed when only **BCP**[18] was employed (ca. 450 nm). On the basis of these observations, and our knowledge of the relative rates of addition of the linear and brush BCPs, it would appear that considerably more linear BCP is incorporated during the initial period of micelle growth. After 2 h, however, it is the incorporation of the brush BCP that begins to determine the growth rate. As a consequence of this mechanism, we would expect the micelles formed during the coassembly of these two unimers to have a gradient structure in which the coronal composition favors the linear block nearest to the seed micelles and the brush block nearest to the termini. To test this hypothesis, each of the brush BCPs were coassembled with PFS_{68}-*b*-$PMVS_{670}$ from ∼225 nm seed micelles and drop-cast samples of the resulting solutions stained with OsO_4 vapor to determine the coronal composition. Significantly, and not anticipated from the observations of reaction rate, we found that the addition of a mixture of either **BCP**[12] or **BCP**[18] together with linear PFS_{68}-*b*-$PMVS_{670}$ resulted in micelles that possessed segmented coronas based on TEM and AFM analysis (see Discussion, section 3). There was, nonetheless, a gradient in the size of the alternating brush and PMVS patches observed, with increasing lengths of the former being located toward the end of the micelles, consistent with the aforementioned growth rates (Figure 8).

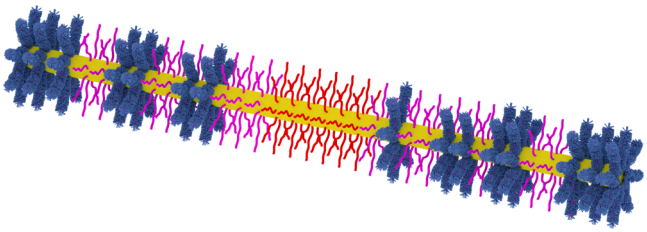

Figure 8. Simplified schematic representation of a block comicelle with segmented coronal domains prepared by the seeded growth of a mixture of PFS_{68}-*b*-$PMVS_{670}$ (pink corona) and **BCP**[18] (blue corona) from a PFS_{60}-*b*-$PDMS_{660}$ seed micelle (red corona).

3. Formation of "Patchy" Coronal Structures. In this study, the presence of segmented coronal structures composed of patches ca. 10−50 nm in size were detected by microscopic analysis of dried coassembled micelle samples involving **BCP**[12] and **BCP**[18]. This feature could either be the consequence of an intrinsic micellar microstructure, as prepared in solution, or might arise during the preparation of samples for microscopy.[62] A distinction between these two possibilities therefore needs to be made before the origin of the phenomenon can be discussed.

Segmented coronas that can be visualized microscopically in the dry-state have previously been prepared by selective solvation of different coronal blocks.[14,63,64] This effect is unlikely to account for the observed segmentation in the present work, however, as *n*-hexane is expected to be a good solvent for both the PMVS and the *n*-alkyl grafted brush blocks. In addition, a previous study has shown no detectable coronal segmentation by TEM in a sample of dried cylindrical comicelles derived from the living CDSA of mixtures of PFS-*b*-PI and PFS-*b*-PDMS unimers from PFS-*b*-PI seed micelles.[53] As the Flory−Huggins interaction parameter $\chi_{(PI-PDMS)}$ in this case is substantially positive (0.13 at 273 K),[65] the results suggest that the observed coronal segmentation in the present study is unlikely to arise from phase segregation of homogeneous or near homogeneous coronas, as the value of $\chi_{(brush\text{-}PMVS)}$ is likely to be at most comparable, and probably lower. It should also be noted that the T_m of the brush-block in **BCP**[18] is 52 °C (Figure S4, Supporting Information), and that crystallization of the corona might be expected to influence the appearance of micelles derived from this material in the dry state. An AFM image of a micelle grown from a PFS_{60}-*b*-$PDMS_{660}$ seed by addition of only **BCP**[18] unimer, however, did not indicate coronal segmentation in the blocks derived from the latter (Figure S17, Supporting Information), whereas segmented micelle coronas were observed in the corresponding **BCP**[18]/PFS_{68}-*b*-$PMVS_{670}$ comicelles under similar conditions. Although drying, selective solvation, and crystallization effects cannot be completely ruled out in the absence of in situ studies, it appears most likely that the segmented corona observed for the comicelles prepared from **BCP**[12] or **BCP**[18] and PFS-*b*-PMVS arises from an underlying segmentation in the micelle structure.

The growth of cylindrical micelles by living CDSA has previously been likened to that of a covalent polymer in a classical living polymerization.[49] It therefore appeared appropriate to investigate whether further similarities could be drawn between the growth of the comicelles in this study and a classical chain-growth copolymerization and, specifically, whether the mechanism for the latter process could be used to account for the segmented micellar structure that appears to be responsible for the observed coronal morphology.

The application of kinetic and statistical considerations has enabled mathematical relationships to be developed that are able to predict the sequence length distribution within a given copolymer.[66] This quantity indicates the probability of finding a segment with $x - 1$ adjacent monomers of the same type, $(N_1)_x$, and will likewise yield information regarding that of adjacent unimers in a comicelle, say, $(N_{PMVS})_x$. These values are derived from the rates of the constituent processes and the molar fractions of monomer or unimer in the feed. In the case of BCP self-assembly, the rate of addition of one PFS_{68}-*b*-$PMVS_{670}$ unimer to a PFS_{68}-*b*-$PMVS_{670}$ terminus, $R_{PMVS-PMVS}$, will be greater than that of the same process involving **BCP**[18], $R_{BCP18\text{-}BCP18}$ (see Discussion, section 1). By the same reasoning, the rate of the switching process (adding one **BCP**[18] unimer to a PFS_{68}-*b*-$PMVS_{670}$ terminus, $R_{PMVS\text{-}BCP18}$, and vice versa, $R_{BCP18\text{-}PMVS}$) will be intermediate between those that lead to the growth of either type of segment. This situation is analogous to the early stages (i.e., low monomer conversion) of a statistical copolymerization where one reactivity ratio, r_{PMVS}, is greater than unity and the other, r_{BCP18}, is less than one.

Unfortunately, the sequence length distribution considers the entity (polymer or micelle) as a whole and does not reflect changes that occur with distance from either the seed or initiator. It therefore cannot readily be used to explain the gradient structure that we observe. Furthermore, if we allow the composition of the feed to vary with conversion of monomer or unimer, as is the case in this study, then certain assumptions in the model no longer hold true, and it becomes nontrivial to extract the sequence length distribution. As a result of these considerations, we resorted to a series of simple simulations to model the addition of linear and brush-block BCP unimer to a

single terminus of a seed micelle. Starting with equimolar amounts of unimer, and relative reaction rates of $R_{linear-linear}$, $R_{brush-brush}$, and $R_{linear-brush}$ or $R_{brush-linear}$ of 6.0, 1.0, and 1.1, respectively, a segment length distribution was obtained that contained 11% of PMVS-containing segments that were greater than eight unimers long (Figure S18, Supporting Information). Such segments would have a length of ca. 5 nm,[67] which suggests that this model for the comicellization of BCP unimers can account for the coronal structure detected by TEM and AFM.

Nevertheless, detailed inspection of the simulation results exposed some differences to the observed micellar structures. Most notably, it was not possible to replicate the large observed gradient in patch size with length from the seed, using any realistic combination of the relative rates. The first-order Markov or terminal model for statistical copolymerizations, however, only considers the effect of the chain terminus on the polymerization rate, whereas we have concluded (see Discussion section 1) that there must also be a *cumulative* effect, arising from coronal steric build up, on the rate of addition when successive brush BCPs are incorporated into a micelle. We therefore repeated the simulation but with an added factor that reduced $R_{brush-brush}$ by a factor 0.67 for each brush BCP unimer that had previously been incorporated into the segment (Figure S19, Supporting Information). This indeed increased the size of the linear BCP segments that were formed closest to the seed and also, necessarily, the size of those arising from the brush block BCP at the terminus. The structure predicted by this simulation, which is based upon a statistical copolymerization model that was modified to account for nearest neighbor effects, would appear to be in good agreement with the experimentally observed structures. It therefore demonstrates that the segmented coronal structure observed could simply arise from the different CDSA rates of the linear and brush block BCPs together with the cumulative effect resulting from steric hindrance associated with the brush block, affording a micelle with an underlying segmented structure (Figure 8).

The model based on the copolymerization of covalent monomers for the coassembly of crystalline-coil BCPs also provides a possible explanation for the observed comicelle structures resulting from the coassembly of linear block copolymers PFS-*b*-PMVS and PFS-*b*-PDMS, and the aforementioned results from the living CDSA of mixtures of PFS-*b*-PI and PFS-*b*-PDMS unimers.[53] In both cases cylindrical micelles without any significant "patchy" coronal segmentation were formed. As all of the aforementioned BCPs were linear, no significant differentiation in CDSA rates would be expected. These processes were therefore simulated as "ideal" copolymerizations where the addition rates for all combinations of added unimer and micelle terminus were equal (Figure S20, Supporting Information). Under these conditions, only 0.5% of PFS-*b*-PMVS chains were contained in segments of greater than 8 unimers in length. In keeping with the experimental results, this situation would be expected to afford micellar structures that would exhibit microscopically homogeneous coronas, or in ideal cases, uniformly distributed fine bands of high and low contrast by TEM when cast from good solvents for both coronal blocks (Figure S14, Supporting Information).

As discussed earlier, "patchy" coronas have previously been detected in cylindrical micelles and block comicelles prepared by the living CDSA of PS-*b*-PE-*b*-PMMA triblock terpolymers with a central crystallizable PE block.[27−29] In this case, however, small-angle neutron scattering (SANS) has verified that such structures exist in solution and are not the consequence of drying effects.[68] Nonetheless, their formation cannot be explained by the copolymerization mechanism invoked in this work because of the identical nature of the building blocks involved. It is perhaps noteworthy that seeded growth in the PS-*b*-PE-*b*-PMMA experiments was considerably slower than that observed with PFS-*b*-PMVS in this work (ca. 1 week vs a few hours),[29] despite both unimers having a linear structure. If the relatively slow rate of growth in the former case is the consequence of slow core-crystallization kinetics, it may be possible for coronal interactions, dictated by χN, to preferentially orient an incoming BCP unimer prior to core-crystallization. This provides an alternative mechanism that would allow the energy-minimized, phase-segregated corona to form, as opposed to being kinetically trapped in a higher energy, homogeneous state by rapid core-crystallization.

■ SUMMARY

We have studied the living CDSA of a series of brush BCPs, where increasing the length of the *n*-alkyl side chains was found to hinder the seeded growth of cylindrical micelles. Cylindrical micelles were prepared more rapidly and with controlled length by the coassembly of **BCP^{6}**, **BCP^{12}**, or **BCP^{18}** with linear PFS_{68}-*b*-$PMVS_{670}$ to relieve steric crowding at the termini of the growing micelles. In the case of **BCP^{12}** and **BCP^{18}**, coronal segmentation of the cylindrical micelles was detected by TEM and AFM, where the size and frequency of compartmentalization could be controlled by the type and amount of brush BCP added. Using this approach, we prepared cylindrical block comicelles that were found to possess a gradient structure due to preferential growth of the linear BCP over that of the more sterically demanding brush BCPs.

The observation that the coronas formed in the gradient structures were "patchy" by TEM and AFM analysis of dried samples has several possible explanations. Simulations of the coassembly process were performed based on a purely statistical model derived to account for observed microstructures of statistical copolymers, but modified to consider the effect of unimers that had crystallized adjacent to the micelle termini. The results indicated that the coassembly of unimers with different rates of addition to a seed terminus together with a cumulative steric attenuation effect can naturally generate a segmented, gradient comicelle architecture. The presence of the latter effect therefore represents a strong contender as a potential explanation for the segmented coronal structures observed. However, detailed further experiments are required in solution, such as SANS, to definitively address this issue, and these will be subjects for future work, together with studies of the utility of the controlled micelle architectures that are accessible using CDSA with these and other crystalline-coil BCP systems.[68,69]

■ ASSOCIATED CONTENT

Supporting Information

Additional information as noted in the text. This material is available free of charge via the Internet at http://pubs.acs.org.

■ AUTHOR INFORMATION

Corresponding Authors

ian.manners@bristol.ac.uk

mwinnik@chem.utoronto.ca

g.whittell@bristol.ac.uk

Notes

The authors declare no competing financial interest.
[§]These authors contributed equally to this work.

■ ACKNOWLEDGMENTS

J.R.F. thanks the European Research Council (ERC) for financial support. D.J.L. thanks the Bristol Chemical Synthesis Centre for Doctoral Training, funded by EPSRC (EP/G036764/1), for the provision of a Ph.D. studentship and the ERC for continued financial support. O.E.C.G. notes his affiliation with the Bristol Centre for Functional Nanomaterials. Z.M.H. is grateful to the European Union (EU) for a Marie Curie Postdoctoral Fellowship. M.A.W. thanks the Natural Sciences and Engineering Research Council (NSERC) of Canada for financial support. I.M. thanks the EU for an ERC Advanced Investigator Grant. We also thank Prof. Felix Schacher (U. Jena, Germany) and Dr. Gerald Guerin (U. Toronto) for useful comments. The authors also thank the Electron Microscopy and Scanning Probe Microscopy Unit of the School of Chemistry, University of Bristol for use of their equipment.

■ REFERENCES

(1) Blanazs, A.; Armes, S. P.; Ryan, A. J. *Macromol. Rapid Commun.* **2009**, *30*, 267−277.
(2) Moughton, A. O.; Hillmyer, M. A.; Lodge, T. P. *Macromolecules* **2012**, *45*, 2−19.
(3) Schacher, F. H.; Rupar, P. A.; Manners, I. *Angew. Chem., Int. Ed.* **2012**, *51*, 7898−7921.
(4) Mai, Y.; Eisenberg, A. *Chem. Soc. Rev.* **2012**, *41*, 5969−5985.
(5) Geng, Y.; Dalhaimer, P.; Cai, S.; Tsai, R.; Tewari, M.; Minko, T.; Discher, D. E. *Nat. Nanotechnol.* **2007**, *2*, 249−255.
(6) Miyata, K.; Christie, R. J.; Kataoka, K. *React. Funct. Polym.* **2011**, *71*, 227−234.
(7) Shah, P. N.; Lin, L. Y.; Smolen, J. A.; Tagaev, J. A.; Gunsten, S. P.; Han, D. S.; Heo, G. S.; Li, Y.; Zhang, F.; Zhang, S.; Wright, B. D.; Panzner, M. J.; Youngs, J.; Brody, S. L.; Wooley, K. L.; Cannon, C. L. *ACS Nano* **2013**, *7*, 4977−4987.
(8) Lin, J.; Wang, S.; Huang, P.; Wang, Z.; Chen, S.; Niu, G.; Li, W.; He, J.; Cui, D.; Lu, G.; Chen, X.; Nie, Z. *ACS Nano* **2013**, *7*, 5320−5329.
(9) Thio, Y. S.; Wu, J.; Bates, F. S. *Macromolecules* **2006**, *39*, 7187−7189.
(10) Cao, L.; Massey, J. A.; Winnik, M. A.; Manners, I.; Riethmüller, S.; Banhart, F.; Spatz, J. P.; Möller, M. *Adv. Funct. Mater.* **2003**, *13*, 271−276.
(11) Hayward, R. C.; Pochan, D. J. *Macromolecules* **2010**, *43*, 3577−3584.
(12) Dupont, J.; Liu, G. *Soft Matter* **2010**, *6*, 3654−3661.
(13) Gröschel, A. H.; Schacher, F. H.; Schmalz, H.; Borisov, O. V.; Zhulina, E. B.; Walther, A.; Müller, A. H. E. *Nat. Commun.* **2012**, *3*, 710.
(14) Gröschel, A. H.; Walther, A.; Löbling, T. I.; Schacher, F. H.; Schmalz, H.; Müller, A. H. E. *Nature* **2013**, *503*, 247−251.
(15) Cui, H.; Chen, Z.; Zhong, S.; Wooley, K. L.; Pochan, D. J. *Science* **2007**, *317*, 647−650.
(16) Zhu, J.; Zhang, S.; Zhang, K.; Wang, X.; Mays, J. W.; Wooley, K. L.; Pochan, D. J. *Nat. Commun.* **2013**, *4*, 2297.
(17) Blanazs, A.; Madsen, J.; Battaglia, G.; Ryan, A. J.; Armes, S. P. *J. Am. Chem. Soc.* **2011**, *133*, 16581−16587.
(18) Fielding, L. A.; Derry, M. J.; Ladmiral, V.; Rosselgong, J.; Rodrigues, A. M.; Ratcliffe, L. P. D.; Sugihara, S.; Armes, S. P. *Chem. Sci.* **2013**, *4*, 2081−2087.
(19) Qiao, X. G.; Lansalot, M.; Bourgeat-Lami, E.; Charleux, B. *Macromolecules* **2013**, *46*, 4285−4295.
(20) Charleux, B.; Delaittre, G.; Rieger, J.; D'Agosto, F. *Macromolecules* **2012**, *45*, 6753−6765.
(21) Gädt, T.; Ieong, N. S.; Cambridge, G.; Winnik, M. A.; Manners, I. *Nat. Mater.* **2009**, *8*, 144−150.
(22) Vilgis, T.; Halperin, A. *Macromolecules* **1991**, *24*, 2090−2095.
(23) Massey, J. A.; Temple, K.; Cao, L.; Rharbi, Y.; Raez, J.; Winnik, M. A.; Manners, I. *J. Am. Chem. Soc.* **2000**, *122*, 11577−11584.
(24) Cao, L.; Manners, I.; Winnik, M. A. *Macromolecules* **2002**, *35*, 8258−8260.
(25) Massey, J.; Power, K. N.; Manners, I.; Winnik, M. A. *J. Am. Chem. Soc.* **1998**, *120*, 9533−9540.
(26) Gädt, T.; Schacher, F. H.; McGrath, N.; Winnik, M. A.; Manners, I. *Macromolecules* **2011**, *44*, 3777−3786.
(27) Schmalz, H.; Schmelz, J.; Drechsler, M.; Yuan, J.; Walther, A.; Schweimer, K.; Mihut, A. M. *Macromolecules* **2008**, *41*, 3235−3242.
(28) Schmelz, J.; Karg, M.; Hellweg, T.; Schmalz, H. *ACS Nano* **2011**, *5*, 9523−9534.
(29) Schmelz, J.; Schedl, A. E.; Steinlein, C.; Manners, I.; Schmalz, H. *J. Am. Chem. Soc.* **2012**, *134*, 14217−14225.
(30) Mihut, A. M.; Drechsler, M.; Möller, M.; Ballauff, M. *Macromol. Rapid Commun.* **2010**, *31*, 449−453.
(31) Du, Z.-X.; Xu, J.-T.; Fan, Z.-Q. *Macromolecules* **2007**, *40*, 7633−7637.
(32) He, W.-N.; Zhou, B.; Xu, J.-T.; Du, B.-Y.; Fan, Z.-Q. *Macromolecules* **2012**, *45*, 9768−9778.
(33) Zhang, J.; Wang, L.-Q.; Wang, H.; Tu, K. *Biomacromolecules* **2006**, *7*, 2492−2500.
(34) Petzetakis, N.; Dove, A. P.; O'Reilly, R. K. *Chem. Sci.* **2011**, *2*, 955−960.
(35) Petzetakis, N.; Walker, D.; Dove, A. P.; O'Reilly, R. K. *Soft Matter* **2012**, *8*, 7408−7414.
(36) Pitto-Barry, A.; Kirby, N.; Dove, A. P.; O'Reilly, R. K. *Polym. Chem.* **2014**, *5*, 1427−1436.
(37) Lazzari, M.; Scalarone, D.; Vazquez-Vazquez, C.; López-Quintela, M. A. *Macromol. Rapid Commun.* **2008**, *29*, 352−357.
(38) Patra, S.; Ahmed, R.; Whittell, G. R.; Lunn, D. J.; Dunphy, E. L.; Winnik, M. A.; Manners, I. *J. Am. Chem. Soc.* **2011**, *133*, 8842−8845.
(39) Gwyther, J.; Gilroy, J. B.; Rupar, P. A.; Lunn, D. J.; Kynaston, E.; Patra, S. K.; Whittell, G. R.; Winnik, M. A.; Manners, I. *Chem.—Eur. J.* **2013**, *19*, 9186−9197.
(40) Lee, I.-H.; Amaladass, P.; Yoon, K.-Y.; Shin, S.; Kim, Y.-J.; Kim, I.; Lee, E.; Choi, T.-L. *J. Am. Chem. Soc.* **2013**, *135*, 17695−17698.
(41) Qian, J.; Li, X.; Lunn, D. J.; Gwyther, J.; Hudson, Z. M.; Kynaston, E.; Rupar, P. A.; Winnik, M. A.; Manners, I. *J. Am. Chem. Soc.* **2014**, *136*, 4121−4124.
(42) Lee, E.; Hammer, B.; Kim, J.-K.; Page, Z.; Emrick, T.; Hayward, R. C. *J. Am. Chem. Soc.* **2011**, *133*, 10390−10393.
(43) Park, S.-J.; Kang, S.-G.; Fryd, M.; Saven, J. G.; Park, S.-J. *J. Am. Chem. Soc.* **2010**, *132*, 9931−9933.
(44) Kamps, A. C.; Fryd, M.; Park, S.-J. *ACS Nano* **2012**, *6*, 2844−2852.
(45) Kamps, A. C.; Cativo, M. H. M.; Fryd, M.; Park, S.-J. *Macromolecules* **2014**, *47*, 161−164.
(46) Jia, L.; Lévy, D.; Durand, D.; Impéror-Clerc, M.; Cao, A.; Li, M.-H. *Soft Matter* **2011**, *7*, 7395−7403.
(47) Gao, Y.; Li, X.; Hong, L.; Liu, G. *Macromolecules* **2012**, *45*, 1321−1330.
(48) Wang, X.; Guerin, G.; Wang, H.; Wang, Y.; Manners, I.; Winnik, M. A. *Science* **2007**, *317*, 644−647.
(49) Gilroy, J. B.; Gädt, T.; Whittell, G. R.; Chabanne, L.; Mitchels, J. M.; Richardson, R. M.; Winnik, M. A.; Manners, I. *Nat. Chem.* **2010**, *2*, 566−570.
(50) Hudson, Z. M.; Lunn, D. J.; Winnik, M. A.; Manners, I. *Nat. Commun.* **2014**, *5*, 3372.
(51) Schmelz, J.; Schacher, F. H.; Schmalz, H. *Soft Matter* **2013**, *9*, 2101−2107.
(52) Schmalz, H.; Schmelz, J.; Drechsler, M.; Yuan, J.; Walther, A.; Schweimer, K.; Mihut, A. M. *Macromolecules* **2008**, *41*, 3235−3242.
(53) Cambridge, G.; Guerin, G.; Manners, I.; Winnik, M. A. *Macromol. Rapid Commun.* **2010**, *31*, 934−938.

(54) Stals, P. J. M.; Li, Y.; Burdyńska, J.; Nicolaÿ, R.; Nese, A.; Palmans, A. R. A.; Meijer, E. W.; Matyjaszewski, K.; Sheiko, S. S. *J. Am. Chem. Soc.* **2013**, *135*, 11421−11424.
(55) Hong, S. W.; Gu, W.; Huh, J.; Sveinbjornsson, B. R.; Jeong, G.; Grubbs, R. H.; Russell, T. P. *ACS Nano* **2013**, *7*, 9684−9692.
(56) Sveinbjörnsson, B. R.; Weitekamp, R. A.; Miyake, G. M.; Xia, Y.; Atwater, H. A.; Grubbs, R. H. *Proc. Natl. Acad. Sci. U. S. A.* **2012**, *109*, 14332−14336.
(57) Bolton, J.; Bailey, T. S.; Rzayev, J. *Nano Lett.* **2011**, *11*, 998−1001.
(58) Lunn, D. J.; Boott, C. E.; Bass, K. E.; Shuttleworth, T. A.; McCreanor, N. G.; Papadouli, S.; Manners, I. *Macromol. Chem. Phys.* **2013**, *214*, 2813−2820.
(59) Previous work has established that the cylindrical micelles with a crystalline PFS core are kinetically trapped structures and that the drying process does not significantly influence their dimensions. See, for example, the results of parallel studies of the growth of cylindrical micelles by CDSA by TEM analysis of dried samples and by light scattering in solution (ref 48). We therefore regard the TEM results we describe as representative of the structures present in solution.
(60) The final L_n values of elongated cylindrical micelles, achieved by addition of equimolar amounts of the two PFS BCPs to the same number of seed micelles, may at first sight be expected to be the same. We note, however, that increasing the coronal chain length can lead to a significant reduction in the linear aggregation number, $N_{agg,\,L}$ (ref 53). We therefore attribute the small difference in the final L_n values of the micelles prepared from PFS_{68}-*b*-$PMVS_{670}$ and **BCP**^{6} to this effect.
(61) The homogeneous nucleation of a series of PFS-based brush BCPs will be the subject of a future study.
(62) It is also likely that the *n*-alkyl branches crystallize within the **BCP**^{18} patches on drying based on the observation of a melting transition for the bulk material by DSC (Figure S4, Supporting Information).
(63) For discussions concerning phase-separation of different coronal chains in micelles and grafted chains on surfaces, see: (a) Hu, J.; Liu, G. *Macromolecules* **2005**, *38*, 8058−8065. (b) Nijikang, G.; Han, D.; Wang, J.; Liu, G. *Macromolecules* **2008**, *41*, 9727−9735. (c) Xiong, D.; Liu, G.; Scott Duncan, E. J. *ACS Appl. Mater. Interfaces* **2012**, *4*, 2445−2454.
(64) Ma, X.; Yang, Y.; Zhu, L.; Zhao, B.; Tang, P.; Qiu, F. *J. Chem. Phys.* **2013**, *139*, 214902−214910.
(65) Alegria, A.; Lund, R.; Barroso-Bujans, F.; Arbe, A.; Colmenero, J. *Colloid Polym. Sci.* **2014**, *292*, 1863−1876.
(66) Odian, G.*Principles of Polymerization*; Wiley-Interscience: Hoboken, NJ, 2004; pp 464−543.
(67) A micelle segment of eight self-assembled BCP units would result in a minimum patch size of 5 nm, if $N_{agg,L}$ is taken as 1.7 nm^{-1} [$8 \times (1.7)^{-1} = 4.8$ nm], see Guérin, G.; Raez, J.; Manners, I.; Winnik, M. A. *Macromolecules* **2005**, *38*, 7819−7827. Features of this size should be readily observable by TEM.
(68) Rosenfeldt, S.; Lüdel, F.; Schulreich, C.; Hellweg, T.; Radulescu, A.; Schmelz, J.; Schmalz, H.; Harnau, L. *Phys. Chem. Chem. Phys.* **2012**, *14*, 12750−12756.
(69) *Self Organized Nanostructures of Amphiphilic Block Copolymers I*; Müller, A. H. E.; Borisov, O., Eds.; Advances in Polymer Science; Springer: Berlin, 2011; Vol. *241*, pp 163−185.